INTERNATIONAL JOURNAL FOR NUMERICAL METHODS IN FLUIDS
Int. J. Numer. Meth. Fluids 2007; **53**:713–733
Published online 23 August 2006 in Wiley InterScience (www.interscience.wiley.com). DOI: 10.1002/fld.1301

Dynamics of large solid particles in bioconvective sedimentation

P. Geng and A. V. Kuznetsov*, †

Department of Mechanical & Aerospace Engineering, North Carolina State University, Box 7910, Raleigh, NC 27695-7910, U.S.A.

SUMMARY

Settling of one or two large solid particles in a bioconvection flow induced by gyrotactic motile microorganisms is investigated using a 2D numerical model. The results of varying the initial positions of large particles on the bioconvection flow pattern are investigated. The Chimera method is utilized to generate subgrids around the moving particles. It is demonstrated that the introduction of a single large particle displaces bioconvection plume and changes its shape. The introduction of two particles on the same side of the bioconvection plume further displaces the plume while the introduction of two particles on opposite sides reduces this displacement. The influence of the bioconvection plume on the particles' settling paths and particles' settling velocities is investigated. Copyright © 2006 John Wiley & Sons, Ltd.

Received 9 March 2006; Revised 24 May 2006; Accepted 26 May 2006

KEY WORDS: bioconvection; Chimera method; large particles; motile microorganisms; moving boundary; streamfunction-vorticity formulation; subgrid; counter-propagating jets

1. INTRODUCTION

Bioconvection caused by gyrotactic microorganisms has been studied extensively, both experimentally and numerically. Bioconvection provides a method for manipulating mass transfer and inducing mixing in microvolumes of fluids that has potential pharmaceutical and bio-technological applications (the importance of mixing in microfluidics is reviewed in Reference [1]). The results of this paper bring to light the interaction between large particles and a bioconvection plume which may be utilized in controlling sedimentation in microvolumes. Possible biomedical link of this research is using bioconvection for faster dissolving of solid particles.

*Correspondence to: A. V. Kuznetsov, Department of Mechanical & Aerospace Engineering, North Carolina State University, Box 7910, Raleigh, NC 27695-7910, U.S.A.
†E-mail: avkuznet@eos.ncsu.edu

Contract/grant sponsor: NASA Office of Biological and Physical Research; contract/grant number: NAG3-2706

Bioconvection is a phenomenon in which physical laws that govern smaller scales lead to a phenomenon visible on a larger scale. While superfluidity and superconductivity are quantum phenomena visible at the macroscale, bioconvection is a mesoscale phenomenon, in which the motion of motile microorganisms induces a macroscopic motion in the fluid. Gyrotactic microorganisms, such as *Dunaliella*, *Chlamydomonas*, *Volvox*, and *Peridinium* [2], swim in a particular direction due to the balance of gravitational and viscous torques. Gyrotactic behaviour causes these microorganisms to accumulate in the regions of most rapid downflow. Since these microorganisms are typically 3–5% heavier than water, the density of the suspension in the regions of downflow becomes larger than in the regions of upflow. Buoyancy increases velocity fluctuations in both upflow and downflow regions thus introducing a hydrodynamic instability [2–4]. The induced convection fluid motion causes the development of bioconvection plumes.

Substantial research into sedimentation has been conducted. For large particles, sedimentation velocity is related to wall separation distances [5]. In Reference [6] particle sedimentation and rotation near a wall is simulated. Particle–particle interactions during sedimentation are studied in Reference [7]. Singh and Joseph [8] extend the numerical research of particle sedimentation to three dimensions. Gan *et al*. [9] present a direct numerical simulation of sedimentation in a flow field induced by natural convection.

Preliminary research has been conducted involving the combined bioconvection-sedimentation problem (called here bioconvective sedimentation). Geng and Kuznetsov [10, 11] investigate the sedimentation of small solid particles in bioconvection. Sedimentation of a single large particle during bioconvection is studied in Reference [12].

This paper investigates sedimentation of one and two large particles in a bioconvection plume. The two-dimensional model considers two large circular particles (see Figure 1(a)) settling in a chamber in which the bioconvection plume is fully developed. The height of the computational domain is H and its width is L, where L is a typical plume spacing and $\lambda = H/L$ is the aspect ratio of the chamber. This paper uses $\lambda = 2$.

The stream function-vorticity method used here is applied to a multi-connected domain that involves moving particles. In order to overcome the complication of imposing boundary conditions at moving boundaries a method similar to that used in Reference [13] is incorporated. The multiple and moving grid systems (see Figures 1(b) and (c)) are formulated using the Chimera method [14, 15].

2. GOVERNING EQUATIONS

2.1. Dimensional governing equations

Governing equations for a bioconvection plume caused by gyrotactic microorganisms are given in References [3, 4] as:

Momentum equation:

$$\rho_0 \left(\frac{\partial \mathbf{V}}{\partial t} + (\mathbf{V} \cdot \nabla)\mathbf{V} \right) = -\nabla p_e + \mu \nabla^2 \mathbf{V} + n_{\mathrm{m}} \theta_{\mathrm{m}} \Delta \rho_{\mathrm{m}} \mathbf{g} \tag{1}$$

Continuity equation:

$$\nabla \cdot \mathbf{V} = 0 \tag{2}$$

DOI: 10.1002/fld

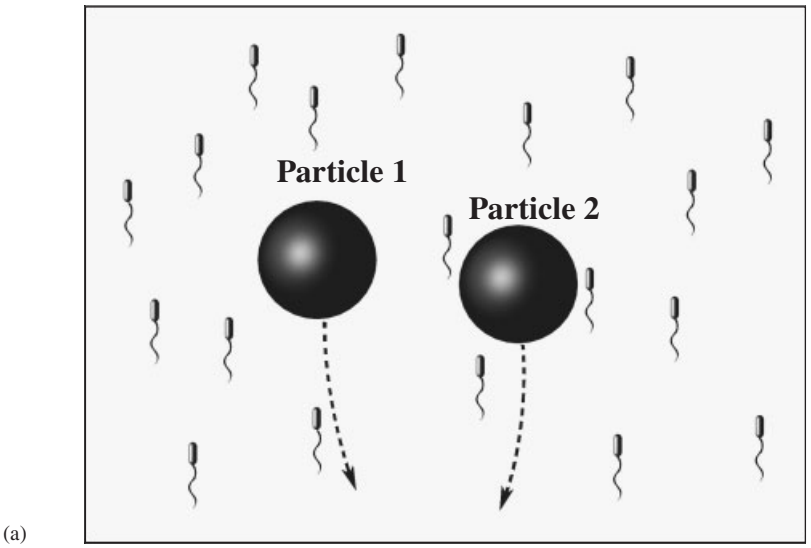

(a)

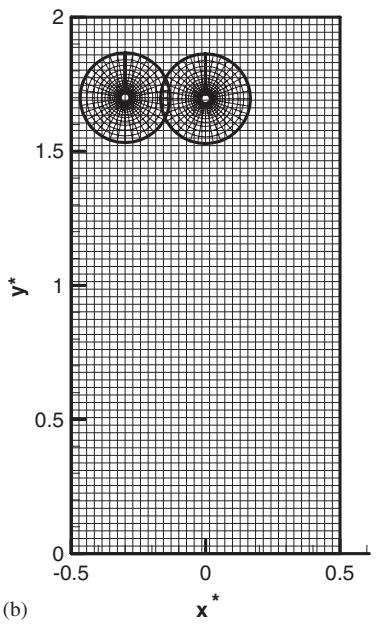

(b)

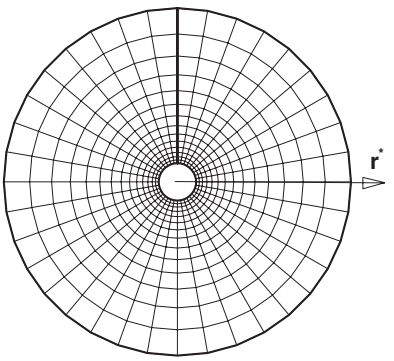

(c)

Figure 1. (a) Schematic diagram of two large particles settling in a bioconvection flow; (b) Chimera grid system, global and subgrid meshes; and (c) Chimera grid system, subgrid mesh.

DOI: 10.1002/fld

Conservation of motile microorganisms:

$$\frac{\partial(n_{\mathrm{m}})}{\partial t} = -\mathrm{div}(n_{\mathrm{m}}\mathbf{V} + n_{\mathrm{m}}W_{\mathrm{m}}\hat{\mathbf{p}} - D_{\mathrm{m}}\nabla n_{\mathrm{m}}) \tag{3}$$

where D_{m} is the diffusivity of microorganisms (it is assumed that all random motions of microorganisms can be approximated by a diffusive process); $\mathbf{g}$ is the gravity vector; n_{m} is the number density of motile microorganisms; $\hat{\mathbf{p}}$ is the unit vector indicating the direction of microorganisms' swimming (equations for this vector are obtained in Reference [2]); p_{e} is the excess pressure (above hydrostatic); $\mathbf{V}$ is the velocity vector, (u, v); t is the time; $W_{\mathrm{m}}\hat{\mathbf{p}}$ is the vector of microorganisms' average swimming velocity (W_{m} is assumed to be constant); $\Delta\rho_{\mathrm{m}}$ is the density difference between microorganisms and water, $\rho_{\mathrm{m}} - \rho_0$; θ_{m} is the volume of a microorganism; μ is the dynamic viscosity of the suspension, assumed to be approximately the same as that of water; and ρ_0 is the density of water.

Applying the second Newton's law to particles, the motion of particles can be described by Equations (4a) and (4b):

$$m_{\mathrm{p}}\frac{\mathrm{d}V_x}{\mathrm{d}t} = F_x, \quad m_{\mathrm{p}}\frac{\mathrm{d}V_y}{\mathrm{d}t} = F_y, \quad I\frac{\mathrm{d}\boldsymbol{\omega}}{\mathrm{d}t} = \mathbf{T} \tag{4a}$$

where $\mathbf{F} = (F_x, F_y)$ is the total external force on a particle, $I = m_{\mathrm{p}}(d^2/8)$ is the polar moment of inertia of a particle, $m_{\mathrm{p}} = \rho_{\mathrm{p}}(\pi d^2/4)$ is the mass of a particle (d is the diameter of a particle), $\mathbf{T}$ is the mechanical torque on a particle, and $\boldsymbol{\omega}$ is the particle's angular velocity vector.

$$\frac{\mathrm{d}x_p}{\mathrm{d}t} = V_x, \quad \frac{\mathrm{d}y_p}{\mathrm{d}t} = V_y, \quad \frac{\mathrm{d}\theta}{\mathrm{d}t} = \omega \tag{4b}$$

where ω is the particle's angular velocity and x_p and y_p are coordinates of particle's centre.

In this research, the two particles are assumed to be of identical mass and size. Particle density is uniform so that the particle geometrical centre is also its centre of mass.

The fluid exerts viscous and pressure forces on the surface of the particles. Since particles are symmetric, the viscous friction on the surface of a particle provides the only contribution to the torque:

$$F_x = \int_{\Omega}\left(\mu\frac{\partial\mathbf{V}_\tau}{\partial\mathbf{n}} - p\mathbf{n}\right)\cdot\hat{\mathbf{x}}\,\mathrm{d}s \tag{5a}$$

$$F_y = \int_{\Omega}\left(\mu\frac{\partial\mathbf{V}_\tau}{\partial\mathbf{n}} - p\mathbf{n}\right)\cdot\hat{\mathbf{y}}\,\mathrm{d}s + \frac{\rho_{\mathrm{p}} - \rho_0}{\rho_{\mathrm{p}}}(\pi d^2/4)\mathbf{g} \tag{5b}$$

$$T = \int_{\Omega}\left(\mu\frac{\partial\mathbf{V}_\tau}{\partial\mathbf{n}}\cdot\frac{d}{2}\right)\mathrm{d}s \tag{5c}$$

where p is the pressure on the surface of the particle, $\mathbf{V}_\tau$ is the tangential fluid velocity along the surface of a particle, and Ω is the surface of a particle.

DOI: 10.1002/fld

2.2. Dimensionless governing equations

The governing equations are recast into the following dimensionless form by utilizing the streamfunction-vorticity formulation:

$$\zeta^* = -\nabla^2 \psi^* \tag{6}$$

$$S_c^{-1}\left(\frac{\partial \zeta^*}{\partial t^*} + u^* \frac{\partial \zeta^*}{\partial x^*} + v^* \frac{\partial \zeta^*}{\partial y^*}\right) = \nabla^2 \zeta^* - \left(R_\mathrm{m} \frac{\partial n_\mathrm{m}^*}{\partial x^*}\right) \tag{7}$$

$$\frac{\partial n_\mathrm{m}^*}{\partial t^*} = -\nabla \cdot [n_\mathrm{m}^*(\mathbf{V}^* + W_\mathrm{m}^* \hat{\mathbf{p}}) - \nabla n_\mathrm{m}^*] \tag{8}$$

The dimensionless variables in Equations (6)–(8) are defined as:

$$\begin{gathered} x^* = \frac{x}{L}, \quad y^* = \frac{y}{L}, \quad t^* = \frac{D_\mathrm{m}}{L^2} t, \quad u^* = \frac{\partial \psi^*}{\partial y^*}, \quad v^* = -\frac{\partial \psi^*}{\partial x^*}, \quad \mathbf{V}^* = \mathbf{V} \frac{L}{D_\mathrm{m}} \\ W_\mathrm{m}^* = W_\mathrm{m} \frac{L}{D_\mathrm{m}}, \quad n_\mathrm{m}^* = \frac{n_\mathrm{m}}{\overline{n}_\mathrm{m}}, \quad S_c = \frac{\nu}{D_\mathrm{m}}, \quad G = \frac{B D_\mathrm{m}}{L^2}, \quad R_\mathrm{m} = \frac{\overline{n}_\mathrm{m} \theta_\mathrm{m} \Delta \rho_\mathrm{m} g L^3}{\rho_0 \nu D_\mathrm{m}} \end{gathered} \tag{9}$$

where G is the gyrotaxis number, R_m is the bioconvection Rayleigh number, S_c is the Schmidt number, ν is the kinematic viscosity of the suspension, and asterisks denote dimensionless quantities.

Microorganisms swim almost vertically upward; since they are gyrotactic (versus being negatively gravitactic, in which case the swimming direction would be strictly vertical), there is a small angle between the direction of their upswimming and the vertical line. For gyrotactic microorganisms, the magnitude of microorganism velocity (10^{-4} m/s is the value used in this paper) is independent of their position and concentration and is determined by species of microorganisms only. By assuming spherical microorganisms and neglecting their inertia, Ghorai and Hill [3, 4] have shown that the vector $\hat{\mathbf{p}}$, which determines the swimming direction of microorganisms, can be computed as:

$$\hat{\mathbf{p}} = \begin{cases} (-\kappa - (\kappa^2 - 1)^{1/2}, 0), & \kappa < -1 \\ (-\kappa, (1 - \kappa^2)^{1/2}), & |\kappa| \leqslant 1 \\ (-\kappa + (\kappa^2 - 1)^{1/2}, 0), & \kappa > 1 \end{cases} \tag{10}$$

where $\kappa = B\zeta = G\zeta^*$. The parameter B is called the 'gyrotactic orientation parameter' by Pedley and Kessler [16]; it is defined as

$$B = \frac{4\pi \mu a^3}{m_\mathrm{m} g h} \tag{11}$$

where a is the radius of a microorganism, h is the displacement of the centre of mass of a gyrotactic microorganism from its centre of buoyancy, and m_m is the mass of a microorganism.

2.3. Initial and boundary conditions

It is assumed that bioconvection plumes occur periodically. The two-dimensional computational domain coincides with a periodic cell that contains a single bioconvection plume. It is assumed

DOI: 10.1002/fld

that the particles do not interact with any bioconvection plumes outside the computational domain. Ghorai and Hill [4] studied the effect of the aspect ratio ($\lambda = H/L$) on bioconvection and found that the steady-state bioconvection plume was stable for $\lambda = 2$. Increasing λ slowed down the solution's convergence to steady state; oscillations were observed for $\lambda = 5$ so that the steady state could never be reached. This paper uses $\lambda = 2$.

The no-slip boundary condition is utilized at the bottom wall. The top and the side boundaries of the computational domain are assumed impermeable to the fluid and stress-free. The top surface of the computational domain is assumed undeformed and strictly horizontal during the sedimentation process.

It is assumed that there is no adhesion between microorganisms and the surface of the particles. For this reason, there is no need to postulate zero relative velocity between microorganisms and the particle surface; it is assumed that microorganisms keep swimming regardless of the distance between the microorganisms and the particle surface. Furthermore, the continuum model of bioconvection utilized in this research does not include a separate momentum equation for microorganisms; therefore, mathematically such condition is not possible within the framework of this model. It is possible, in principal, to develop a mesoscale model of bioconvection, which would track the motion of every single microorganism and hence consider momentum conservation for each microorganism. Such model could include a more detailed treatment of interactions between microorganisms and the surface of the particle. However, in a typical dilute suspension there are 10^6 microorganisms in 1 cm^3 of the suspension, which would make such computations impractical.

Under these assumptions, the boundary conditions for the computational domain can be presented as:

$$\psi^* = 0 \quad \text{at } y^* = 0, \lambda \quad \text{and} \quad x^* = \pm 0.5 \tag{12a}$$

$$\frac{\partial \psi^*}{\partial y^*} = 0 \quad \text{at } y^* = 0 \tag{12b}$$

$$\frac{\partial^2 \psi^*}{\partial y^{*2}} = 0 \quad \text{at } y^* = \lambda \quad \text{and} \quad \frac{\partial^2 \psi^*}{\partial x^{*2}} = 0 \quad \text{at } x^* = \pm 0.5 \tag{12c}$$

Normal fluxes of microorganisms are zero through all boundaries of the computational domain and the surfaces of the moving particles:

$$\mathbf{J}^*_{\mathrm{m}} \cdot \hat{\mathbf{y}} = 0 \quad \text{at } y^* = 0, \lambda, \quad \mathbf{J}^*_{\mathrm{m}} \cdot \hat{\mathbf{x}} = 0 \quad \text{at } x^* = \pm 0.5 \tag{13a}$$

$$\mathbf{J}^*_{\mathrm{m}} \cdot \hat{\mathbf{r}} = 0 \text{ at the surface of a moving particle} \tag{13b}$$

where $\hat{\mathbf{x}}$, $\hat{\mathbf{y}}$, and $\hat{\mathbf{r}}$ are the unit vectors in the x-, y-, and r-directions, respectively, and

$$\mathbf{J}^*_{\mathrm{m}} = n^*_{\mathrm{m}}(\mathbf{V}^* + W^*_{\mathrm{m}}\hat{\mathbf{p}}) - \nabla n^*_{\mathrm{m}} \tag{14}$$

is the dimensionless flux of microorganisms.

The streamfunction and vorticity are defined in the polar coordinate system for the subgrids created around the particles as follows:

$$\zeta^* = -\left(\frac{\partial^2 \psi^*}{\partial r^{*2}} + \frac{1}{r^*}\frac{\partial \psi^*}{\partial r^*} + \frac{1}{r^{*2}}\frac{\partial^2 \psi^*}{\partial \theta^2}\right) \tag{15}$$

DOI: 10.1002/fld

$$V_r^* = \frac{1}{r^*}\frac{\partial \psi^*}{\partial \theta}, \quad V_\theta^* = -\frac{\partial \psi^*}{\partial r^*} \tag{16}$$

where r^* is a dimensionless coordinate used around the particle (see Figure 1(c)), and V_r^* and V_θ^* are the dimensionless velocity components in the polar coordinate system.

At the surface of the settling particles, the no-slip boundary condition is imposed. Geng and Kuznetsov [12] have shown that the values of the streamfunction and vorticity on a moving boundary in a multi-connected domain can be calculated numerically by the following procedure.

Using Taylor series expansion for $\psi^*(r^*, \theta)$ near the moving boundary, $\partial^2\psi^*/\partial\theta^2$ on the particle surface is expressed as

$$\frac{\partial^2 \psi^*}{\partial r^{*2}} = \frac{8\psi^*(1,\theta) - \psi^*(2,\theta) - 7\psi^*(0,\theta) - 6\Delta r(\partial\psi^*/\partial r^*)}{2\Delta r^2} + O((\Delta r)^4) \tag{17}$$

The equation to calculate $\zeta^*(0, \theta)$ on the particle surface is derived by substituting Equation (17) into Equation (15):

$$\zeta^*(0,\theta) = \frac{\left(-6\Delta r + (2(\Delta r)^2/r_0)\right) V_\theta^*(0,\theta) - (8\psi^*(1,\theta) - \psi^*(2,\theta) - 7\psi^*(0,\theta))}{2(\Delta r)^2} - \frac{1}{r_0}\frac{\partial V_r^*}{\partial \theta} \tag{18}$$

where r_0 is the radius of the particle.

To calculate the boundary values of the streamfunction on a moving boundary, Equation (1) is multiplied by a unit tangential vector $\hat{\boldsymbol{\tau}}$ along the surface of a particle. Ignoring the pressure difference along the particle's surface, the following equation for $\psi^*(0, \theta)$ is obtained:

$$\psi^*(0,\theta) = -\frac{4(\Delta r)^3 M - 8(\Delta r)^2\zeta^*(1,\theta) + 2(\Delta r)^2\zeta^*(2,\theta)}{21} + \frac{(6\Delta r - 2[(\Delta r)^2/r_0])V_\theta^*(0,\theta)}{7} + \frac{8}{7}\psi^*(1,\theta) - \frac{1}{7}\psi^*(2,\theta) + \frac{2}{7}\frac{(\Delta r)^2}{r_0}\frac{\partial V_r^*}{\partial \theta} \tag{19}$$

where

$$M = \frac{\partial \zeta^*}{\partial \mathbf{n}} = -\frac{1}{S_c}\left(\frac{\partial \mathbf{V}_\tau^*}{\partial t^*} + (\mathbf{V}^* \cdot \nabla)\mathbf{V}_\tau^*\right) - R_{\mathrm{m}} n_{\mathrm{m}} \hat{\mathbf{y}} \cdot \hat{\boldsymbol{\tau}} \tag{20}$$

Initially, at $t^* = 0$, the bioconvection plume is assumed fully developed. The two particles are released just beneath the free surface to keep all subgrid nodes located inside the computational domain. It is assumed that the particles' initial velocity is zero.

2.4. Numerical procedure

In this paper, following the Chimera method [14], two subgrids are created; one around each particle, and a global rectangular grid is created for the global flow field, as demonstrated in Figures 1(b)

DOI: 10.1002/fld

and (c). Governing Equations (6)–(8) for the global grid and the two subgrids are solved separately. The exchange of information between the global grid and the subgrids is implemented by interpolation. The unknown boundary values of variables on the subgrids are computed by interpolating these boundary points onto the known global grid. Therefore, the computational problem for the subgrids is transformed to a boundary value problem. The same procedure is required for computations on the global grid except that two artificial unknown inner boundaries (projected onto subgrids) are created around the moving particles.

A conservative finite-difference scheme is utilized to discretize the governing equations in both the Cartesian and polar coordinate systems. An implicit scheme with Euler backward differencing in time and central differencing in space is utilized. A line-by-line tri-diagonal matrix algorithm and an iteration technique with over-relaxation for the number density of microorganisms on the global grid and under-relaxation for other variables for both global and subgrid nodal points is used to solve the discretized equations. A staggered mesh is utilized in which the streamfunction and vorticity are stored in one nodal set while the number density of microorganisms is stored in another nodal set. Computations are performed on a 3.0 GHz Intel Xeon processor. Typical CPU time required to investigate particles settling from just beneath the free surface to near the bottom of the computational domain for a 36×72 uniform global mesh and two 15×36 non-uniform curvilinear meshes is 200 h. It is established that further refinement of the computational meshes does not significantly impact the results.

3. RESULTS AND DISCUSSION

Values of physical properties and dimensionless parameters utilized in computations are summarized in Table I. The parameters of microorganisms are identical to those given in Table I of Reference [4].

Bioconvection flows are characterized by small Reynolds numbers. Reynolds number in bioconvection flows can be defined by several different ways. Kessler [17] defined the Reynolds number as follows:

$$Re_{\mathrm{m}} = \frac{W_{\mathrm{m}} a \rho_0}{\mu} = \frac{(10^{-4}\ \mathrm{m/s})(5 \times 10^{-6}\ \mathrm{m})(10^3\ \mathrm{kg/m^3})}{10^{-3}\ \mathrm{Pa\ s}} = 5 \times 10^{-4}$$

where a is the radius of a microorganism ($= 5 \times 10^{-6}$ m).

If the lengthscale is changed to the particle radius, the Reynolds number is

$$Re_{\mathrm{p}} = \frac{W_{\mathrm{m}} r_0 \rho_0}{\mu} = \frac{(10^{-4}\ \mathrm{m/s})(9 \times 10^{-5}\ \mathrm{m})(10^3\ \mathrm{kg/m^3})}{10^{-3}\ \mathrm{Pa\ s}} = 9 \times 10^{-3}$$

A typical fluid convection velocity in bioconvection can be estimated as twice of W_{m}, so if velocity scale is changed to the maximum fluid velocity, these Reynolds numbers are approximately doubled. In summary, $Re \ll 1$ for any of the above definitions of the Reynolds number.

Four cases with different particle initial positions are investigated. The same initial position ($x^* = -0.3$, $y^* = 1.8$) is used for one particle (denoted Particle 1) in all cases (A–D). In Case A Particle 1 is released by itself while in Cases B–D a second particle (denoted Particle 2) is released

DOI: 10.1002/fld

Table I. Physical properties, geometrical parameters, and values of dimensionless parameters utilized in computations.

Average number density of microorganisms	$\overline{n}_{\mathrm{m}}$	10^{12} cells/m^3
Density of water	ρ_0	10^3 kg/m^3
Density of microorganisms	ρ_{m}	1.05×10^3 kg/m^3
Volume of a microorganism	θ_{m}	5×10^{-16} m^3
Average swimming velocity of microorganisms	W_{m}	10^{-4} m/s
Diffusivity of microorganisms	D_{m}	5×10^{-8} m^2/s
Gyrotaxis orientation parameter	B	5 s
Kinematic viscosity of the suspension	v	10^{-6} m^2/s
Height of the computational domain	H	0.01 m
Width of the computational domain	L	0.005 m
Dimensionless average swimming velocity of microorganisms	$W^*_{\mathrm{m}} = W_{\mathrm{m}} \dfrac{L}{D_{\mathrm{m}}}$	10
Schmidt number	$S_c = \dfrac{v}{D_{\mathrm{m}}}$	20
Gyrotaxis number	$G = \dfrac{B D_{\mathrm{m}}}{L^2}$	10^{-2}
Bioconvection Rayleigh number	$R_{\mathrm{m}} = \dfrac{\overline{n}_{\mathrm{m}} \theta_{\mathrm{m}} \Delta\rho_{\mathrm{m}} g L^3}{\rho_0 v D_{\mathrm{m}}}$	612.5
Aspect ratio of the computational domain	$\lambda = \dfrac{H}{L}$	2
Radius of the particles	r_0	9×10^{-5} m
Density of the particles	ρ_{p}	1.2×10^3 kg/m^3

Table II. Initial positions of particle centres for Cases A–D.

	Case A	Case B	Case C	Case D
Particle 1 (x^*, y^*)	$(-0.3, 1.8)$	$(-0.3, 1.8)$	$(-0.3, 1.8)$	$(-0.3, 1.8)$
Particle 2 (x^*, y^*)	No Particle 2 in Case A	$(-0.1, 1.8)$	$(0.1, 1.8)$	$(0.3, 1.8)$

at varing positions. Positions of centres of the particles at $t = 0$ are summarized in Table II. Particles are released beneath the free surface so that the subgrids are located completely inside the global grid; since the vertical position of the free surface corresponds to $y^* = 2.0$, the centres of the particles are initially located at $y^* = 1.8$.

3.1. No particles

To quantify the influence of particle sedimentation, a purely bioconvection flow pattern is used as a reference (depicted in Figure 2). Figure 2(a) shows the dimensionless number density of microorganisms, Figure 2(b) shows contour lines of the dimensionless vorticity, Figure 2(c) displays contour lines of the dimensionless streamfunction, and Figure 2(d) shows the vector field of the fluid velocity. The bioconvection plume is located in the centre of the computational domain. The

DOI: 10.1002/fld

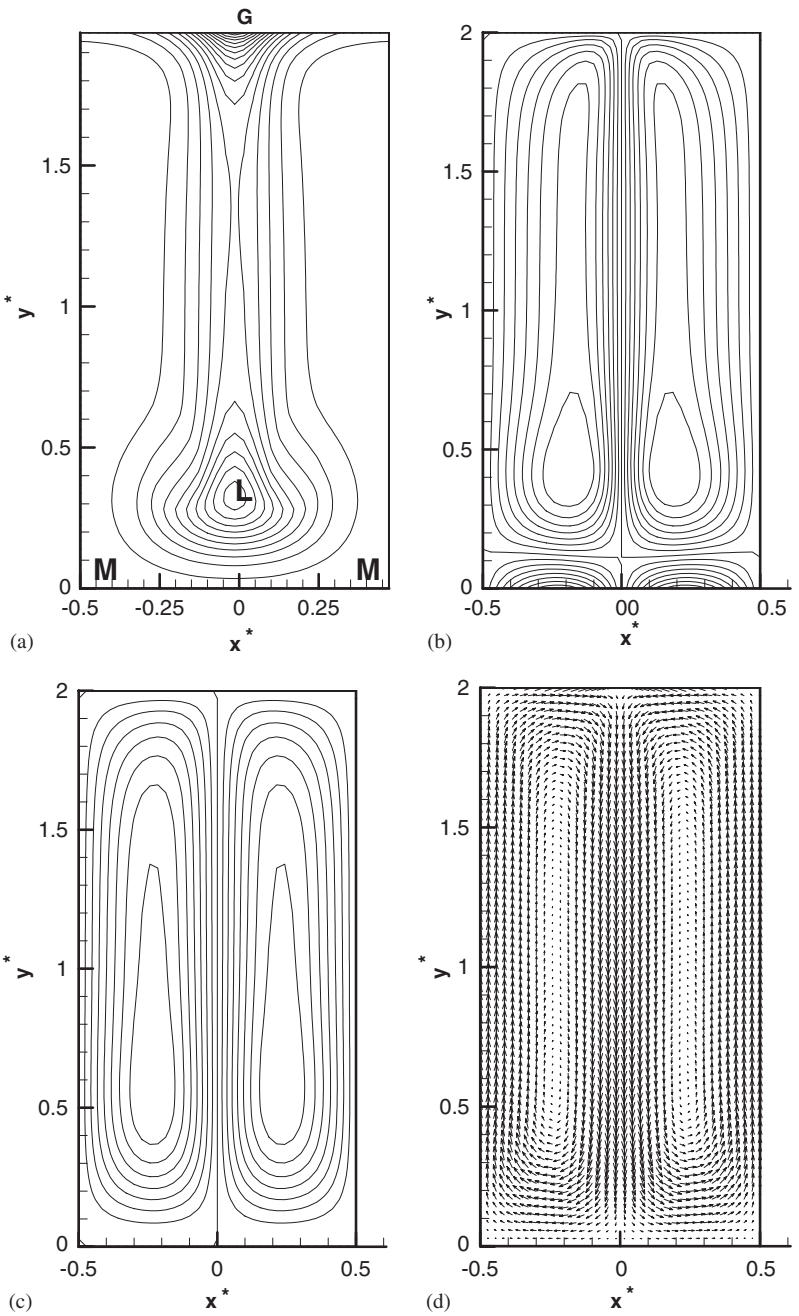

Figure 2. Steady-state bioconvection plume: (a) dimensionless number density of microorganisms; (b) contour lines of the dimensionless vorticity; (c) contour lines of the dimensionless streamfunction; and (d) vector field of fluid velocity.

DOI: 10.1002/fld

number density of microorganisms takes on its maximum value (a *global maximum*) in the center of the free surface (marked by G in Figure 2(a)). The fluid flow is directed downward in the centre of the domain and upward at its periphery, this flow transports microorganisms from the upper fluid layer to the bottom of the domain and causes a *local maximum* of their number density (marked by L in Figure 2(a)). The number density of microorganisms takes on its *minimum* value at the bottom corners of the computational domain (marked by M in Figure 2(a)).

Data presented in Figure 2 are in good agreement with those plotted in Figure 9 of Reference [3].

3.2. Single particle (Case A)

In Case A Particle 1 is released by itself in the bioconvection plume. Figure 3 shows the dimensionless number density of microorganisms, contour lines of the dimensionless vorticity, contour lines of the dimensionless streamfunction, and a vector field of the fluid velocity for Case A 1.0 s after Particle 1 is released. Figure 3(a) shows that the bioconvection plume is displaced away from Particle 1 as the particle settles on the left side of the bioconvection plume. Convective circulations are developed on both sides of the particle. The convective circulation on the right side of the particle is stronger than on the left (see Figures 3(c) and (d)). Comparing Figure 3(a) with Figure 2(a) it is evident that the maximum value of the number density of microorganisms is shifted from the centre of the free surface to the left and is located directly above the particle (the meanings of G, L, and M in Figure 3(a) are the same as that in Figure 2(a)). To the left of the particle in the upper part of the computational domain the fluid velocity is directed downward while in the lower part of the domain the fluid velocity is directed upward (the sheer-free boundary condition used at the domain's side walls implies that the horizontal velocity vanishes but the vertical velocity does not). Counter-propagating vertical jets (marked by block arrows in Figure 3(d)) collide to the left of the particle and create a horizontal jet directed to the right. Figure 7(d) shows that Particle 1 is displaced by this horizontal jet from $x^* = -0.3$ to -0.2 as it settles.

3.3. Multiple particles (Cases B–D)

To see how the two particles affect bioconvection as well as how they influence each other's sedimentation, Particle 2 is released simultaneously with Particle 1. Particle 1 retains the same initial position while the initial position of Particle 2 is varied (see Table II).

In Case B (Figure 4) Particle 2 is also released to the left of the plume (at $x^* = -0.1$). The bioconvection plume is pushed to the right and away from the settling particles. By the end of sedimentation, both particles are displaced from the left side of the computational domain to the centre of the domain. Figure 4(a) shows that at $t = 1.1$ s Particle 2 has a lower vertical position than Particle 1 reflecting a larger downward vertical velocity. This is because the bioconvection velocity is directed downward in the centre of the domain and upward at its periphery. Figure 4(d) ($t = 0.1$ s) shows that convective circulation around Particle 2 is stronger than around Particle 1, so that Particle 1 is displaced to the left in the beginning of the sedimentation process (see Figure 7(a)). In Figure 4(d) ($t = 0.5$ s), similarly to case A, counter-propagating jets develop to the left of Particle 1. The fluid velocity is downward to the left of Particle 1 in the upper part of the computational domain and upward in the lower part of the domain. A horizontal jet develops displacing Particle 1 to the right (as in Case A in Figure 3). Another horizontal jet is generated between the two particles because of the collision of the two vertical counter-propagating jets marked by block arrows in

DOI: 10.1002/fld

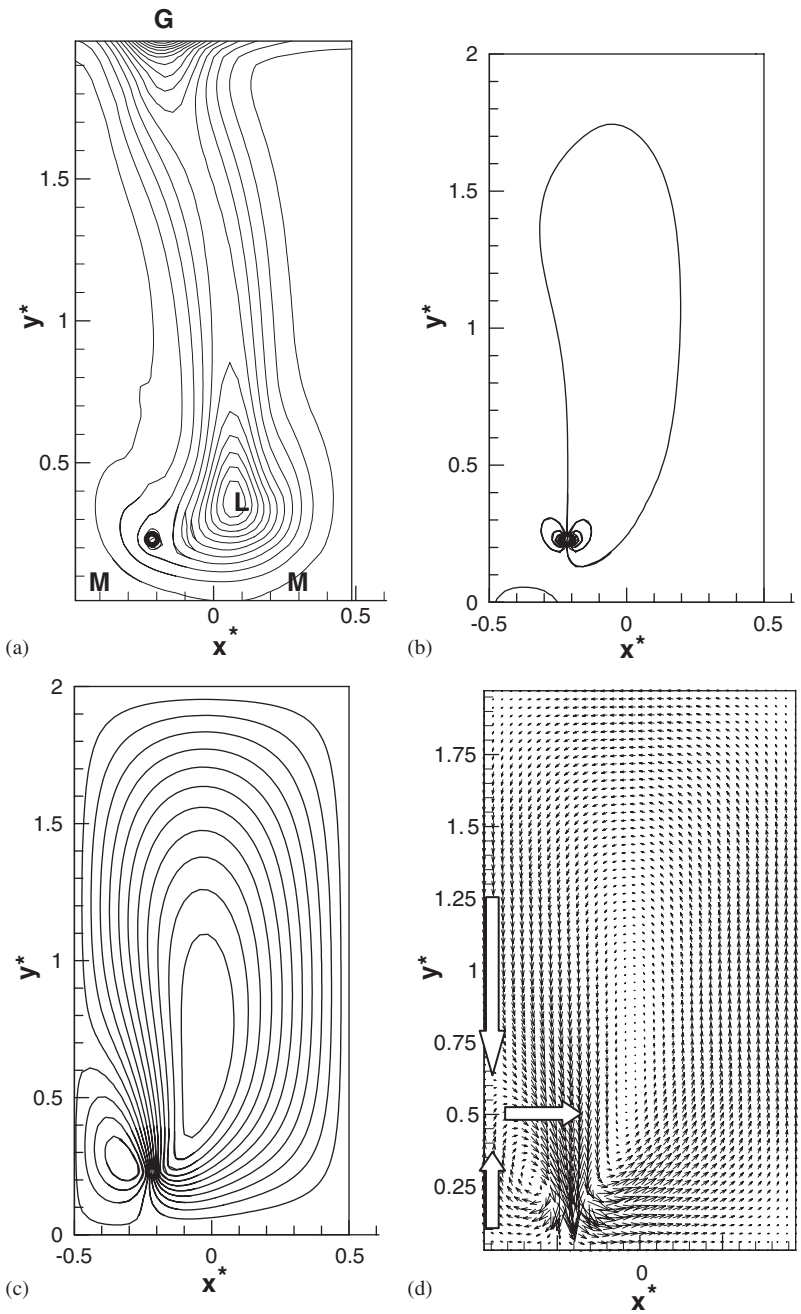

Figure 3. Case A, $t = 1.0$ s: (a) dimensionless number density of microorganisms; (b) contour lines of the dimensionless vorticity; (c) contour lines of the dimensionless streamfunction; and (d) vector field of fluid velocity.

DOI: 10.1002/fld

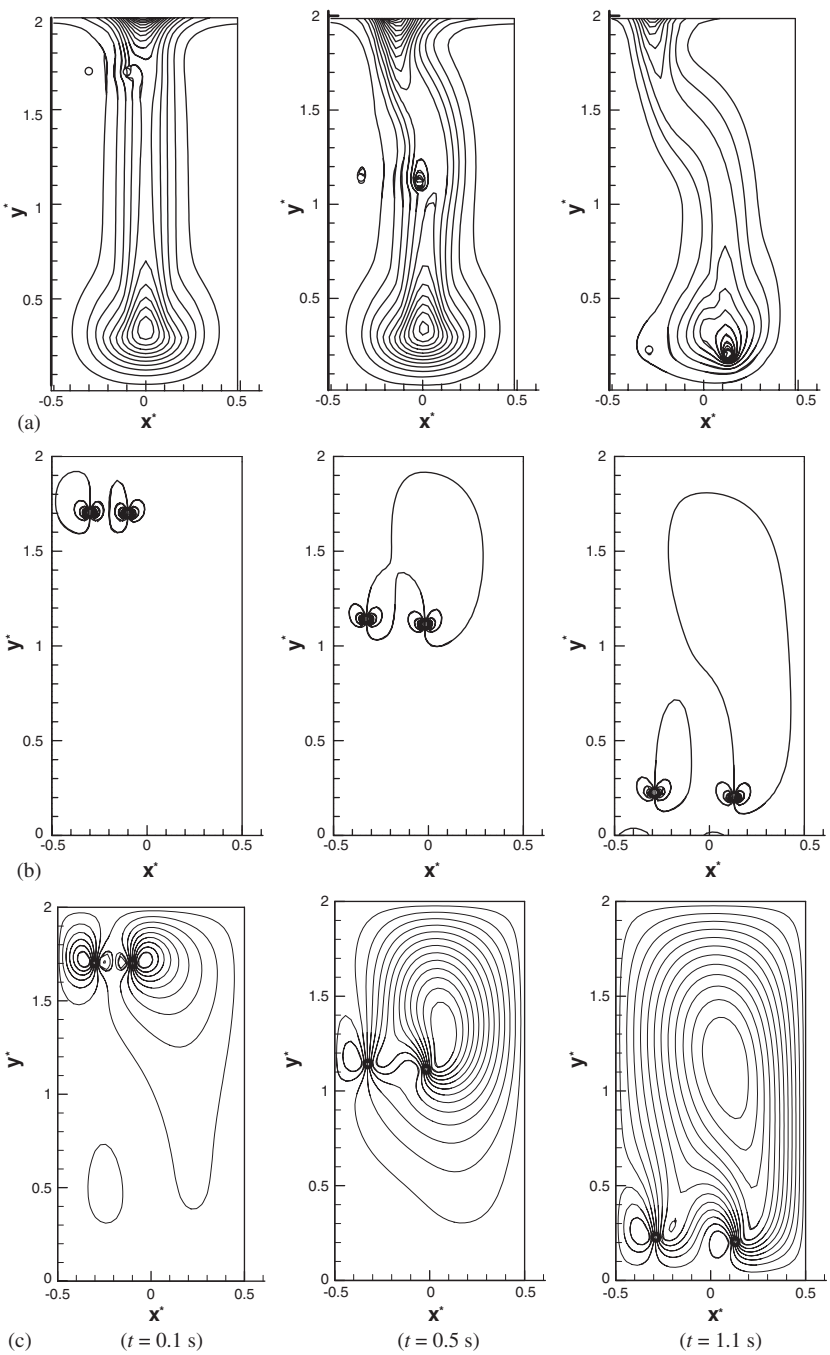

Figure 4. Case B: (a) dimensionless number density of microorganisms; (b) contour lines of the dimensionless vorticity; (c) contour lines of the dimensionless streamfunction, and (d) vector field of fluid velocity.

DOI: 10.1002/fld

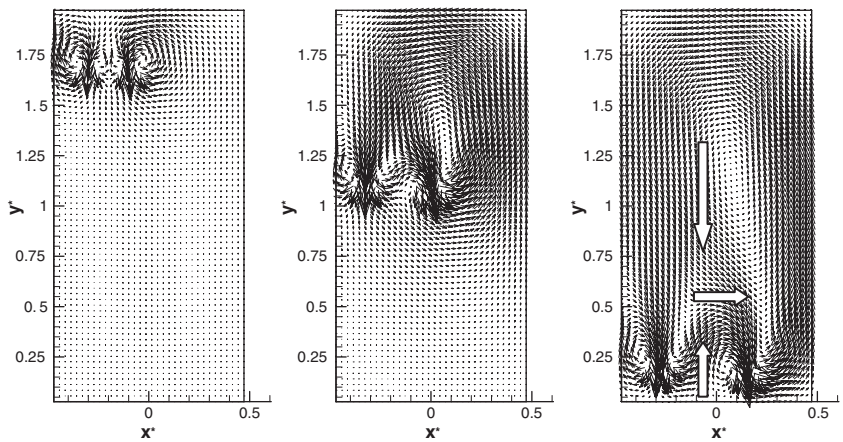

Figure 4. *Continued.*

Figure 4(d) ($t = 1.1$ s). This horizontal jet pushes Particle 2 to the right. The paths of the particle centres for Case B are displayed in Figure 7(a). As explained above, initially Particle 1 is displaced to the left by the convective circulation caused by Particle 2. Later the horizontal jet developed during sedimentation pushes Particle 1 to the right. Particle 2 is displaced to the right during the whole duration of the sedimentation process by the horizontal jet generated between Particles 1 and 2. Comparing Figures 4(a) ($t = 1.1$ s) and 3(a), it is evident that the bioconvection plume has larger horizontal displacement in Case B than in Case A, which means that introducing an additional particle on the same side of the plume increases the displacement of the bioconvection plume.

In Case C (Figure 5), Particle 2 is released to the right of the plume, at $x^* = 0.1$, thus the convective circulations induced by the two particles are more symmetric. Figure 5(a) shows that the displacement of the bioconvection plume to the right is less than in Cases A and B. Particle 1, which is farther away from the centre of the plume than Particle 2, has more effect on the plume displacement, implying a direct relation between particle distance from the plume centre and influence on plume displacement. Obviously, moving the particle far away from the plume will diminish this influence; therefore, it is expected that there exists an optimal distance at which the particle's effect on the plume is the strongest. Both particles move to the right during sedimentation as seen in Figure 7(b). The distance between the particles in Case C is too great for the convection circulation around Particle 2 to have any noticeable effect on Particle 1. Recall that this is not so in Case B (Figure 4(d)) where the particles are closely spaced and the convection circulation around Particle 2 influences Particle 1 by initially displacing it to the left (Figure 7(a)). Particle 2 has larger vertical velocity than Particle 1. The paths of the particle centres for Case C are displayed in Figure 7(b). Particle 2 exhibits larger horizontal displacement than Particle 1 during sedimentation.

In Case D (Figure 6), the two particles are initially positioned symmetrically relative to the vertical centreline of the bioconvection plume, so that for Particle 2, $x^* = 0.3$. Sedimentation occurs symmetrically and the two particles settle without significantly changing the shape and location of the bioconvection plume. Comparing Figure 2 (no particles) and Figure 6(a) ($t = 0.5$ s), it is

DOI: 10.1002/fld

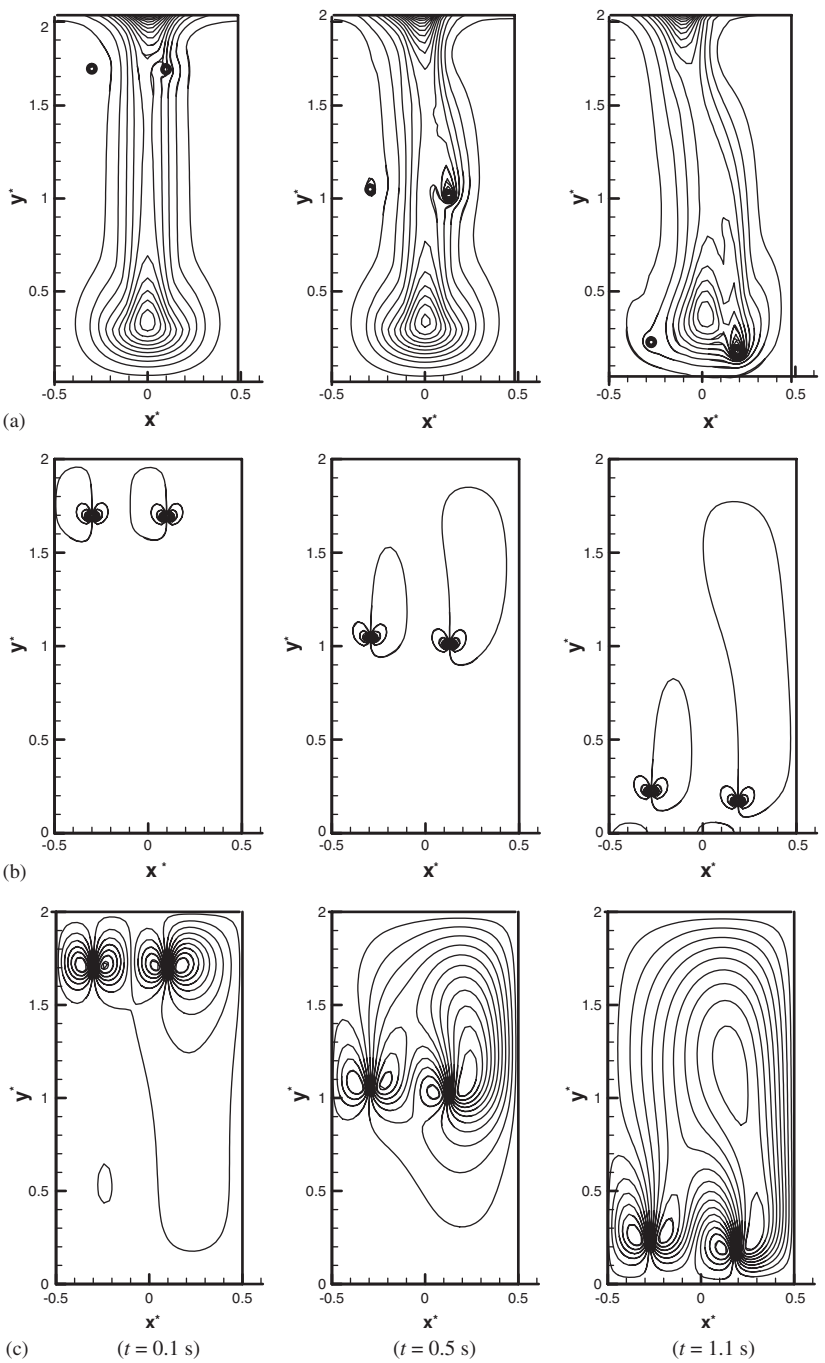

Figure 5. Case C: (a) dimensionless number density of microorganisms; (b) contour lines of the dimensionless vorticity; (c) contour lines of the dimensionless streamfunction; and (d) vector field of fluid velocity.

DOI: 10.1002/fld

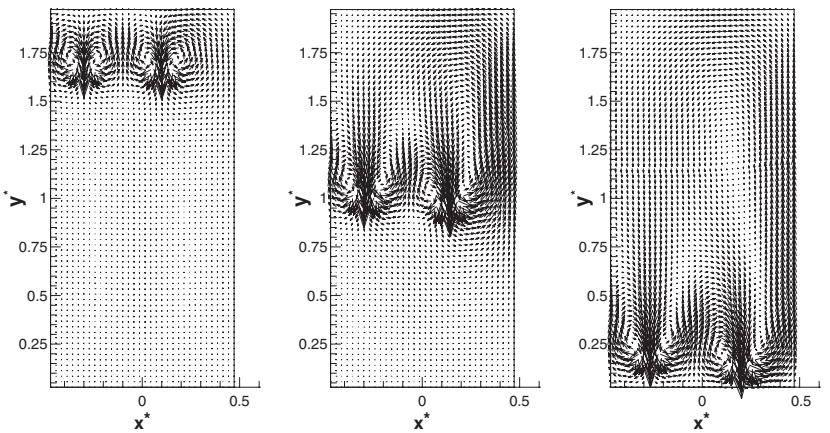

(d) ($t = 0.1$ s) ($t = 0.5$ s) ($t = 1.1$ s)

Figure 5. *Continued.*

evident that the particles have a constructive influence, locally reducing the width of the plume in a horizontal plane where the particles are located. No noticeable horizontal jets are found in Figure 6(d), which means that the horizontal displacements that the two particles exhibit are caused by bioconvection. The paths of particle centres for Case D are displayed in Figure 7(c). The two particles move from the periphery of the domain toward its centre during sedimentation because of bioconvection. The bioconvection flow is directed toward the plume's centre in the upper part the domain and away from the plume's centre in the lower part of the domain. This explains why the particles are displaced toward the centre of the domain during sedimentation, moving first with an increasing horizontal velocity and then with a decreasing horizontal velocity.

The paths of Particle 1 (Cases A–D) are summarized in Figure 7(d). Particle 1 exhibits a large horizontal displacement in Case A while with the addition of Particle 2 in Cases B–D this displacement decreases. The presence of Particle 2 increases the symmetry of convection. The greater the distance between the two particles initially, the less Particle 1's course is altered.

In order to additionally validate numerical results, Figures 8(a) and (b) displays the dimensionless y-velocity, V_y^*, of Particles 1 and 2, respectively, for various cases. The horizontal lines in Figures 8(a) and (b) show the particle terminal velocity resulting from the balance of the gravitational force and drag on the particle:

$$F_D = (\rho_p - \rho_0)(\pi r_0^2)g \tag{21}$$

The particle terminal velocity, U, is found by substituting Equation (21) into the following experimental curve-fit correlation for a drag coefficient in a flow past a circular cylinder suggested by Sucker and Brauer [18]:

$$C_D = \frac{F_D}{\rho_0 U^2 r_0} \approx 1.18 + \frac{6.8}{Re^{0.89}} + \frac{1.96}{Re^{0.5}} - \frac{0.0004Re}{1 + 3.64 \times 10^{-7} Re^2} \tag{22}$$

where $Re = 2Ur_0/\nu$ and F_D is the drag on the cylinder.

DOI: 10.1002/fld

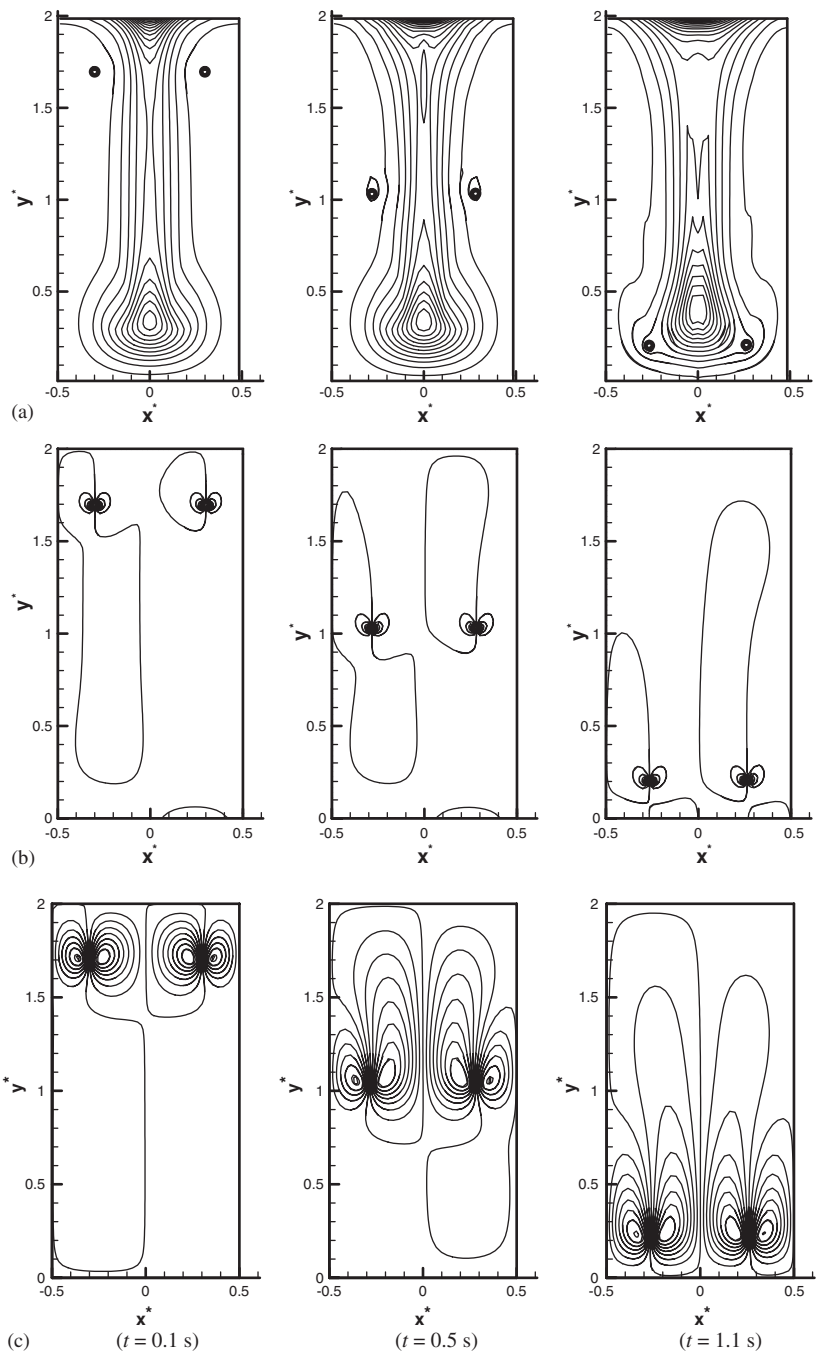

Figure 6. Case D: (a) dimensionless number density of microorganisms; (b) contour lines of the dimensionless vorticity; (c) contour lines of the dimensionless streamfunction; and (d) vector field of fluid velocity.

DOI: 10.1002/fld

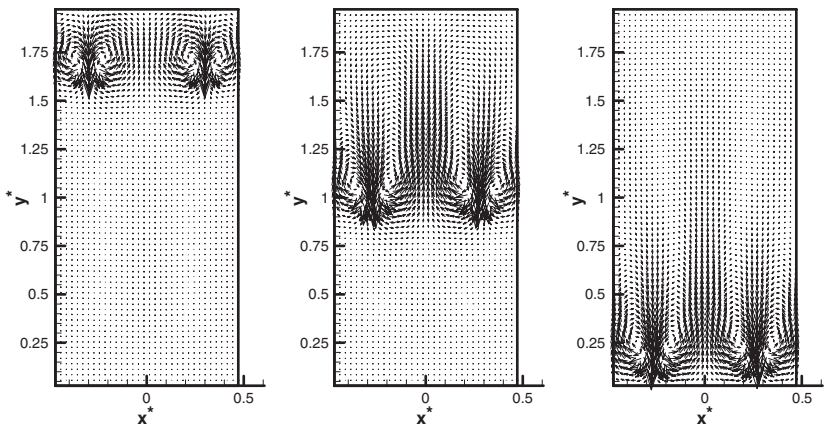

(d) (t = 0.1 s) (t = 0.5 s) (t = 1.1 s)

Figure 6. *Continued.*

Figure 8 shows that particle velocities at the end of the sedimentation process approach the particle terminal velocity (obtained using experimental correlation (22)) in all Cases A–D, which validates the obtained numerical results. The settling velocity of the particles at the end of sedimentation is a little smaller than the particle terminal velocity because the bioconvection flow creates a 'pillow' at the bottom of the chamber and slows down sedimentation. Another reason for slowing down the particle as it approaches the bottom (this reason would exist even if the fluid contained no microorganisms) is that the upflow is required to replace the mass displaced by the sedimenting particle. At the end of sedimentation, the particle velocity of the single particle case (Case A) is closer to U than that of the multiple particle cases (Cases B–D). This is apparently a result of the interaction of the multiple particles with the bioconvection plume.

4. CONCLUSIONS

Sedimentation of one and two large particles suddenly released in a fully developed bioconvection plume is investigated. Particle sedimentation changes the shape and location of the bioconvection plume. Settling of a single particle to one side of the plume shifts the bioconvection plume away from the particle. Increasing geometric similarity about the plume centre for multiple particle sedimentation decreases plume displacement while decreasing this similarity increases plume displacement. The particles' settling is also affected by bioconvection. Because of bioconvection, particles are pushed in both vertical and horizontal directions. The direct interaction between the bioconvection plume and the particles as well as the indirect interaction between the two particles depends on the initial position of the particles. The computational results suggest evidence of an optimal distance between the vertical symmetry plane of the unit cell and the initial position of the particle at which the particle's effect on the plume is the strongest. Further numerical

DOI: 10.1002/fld

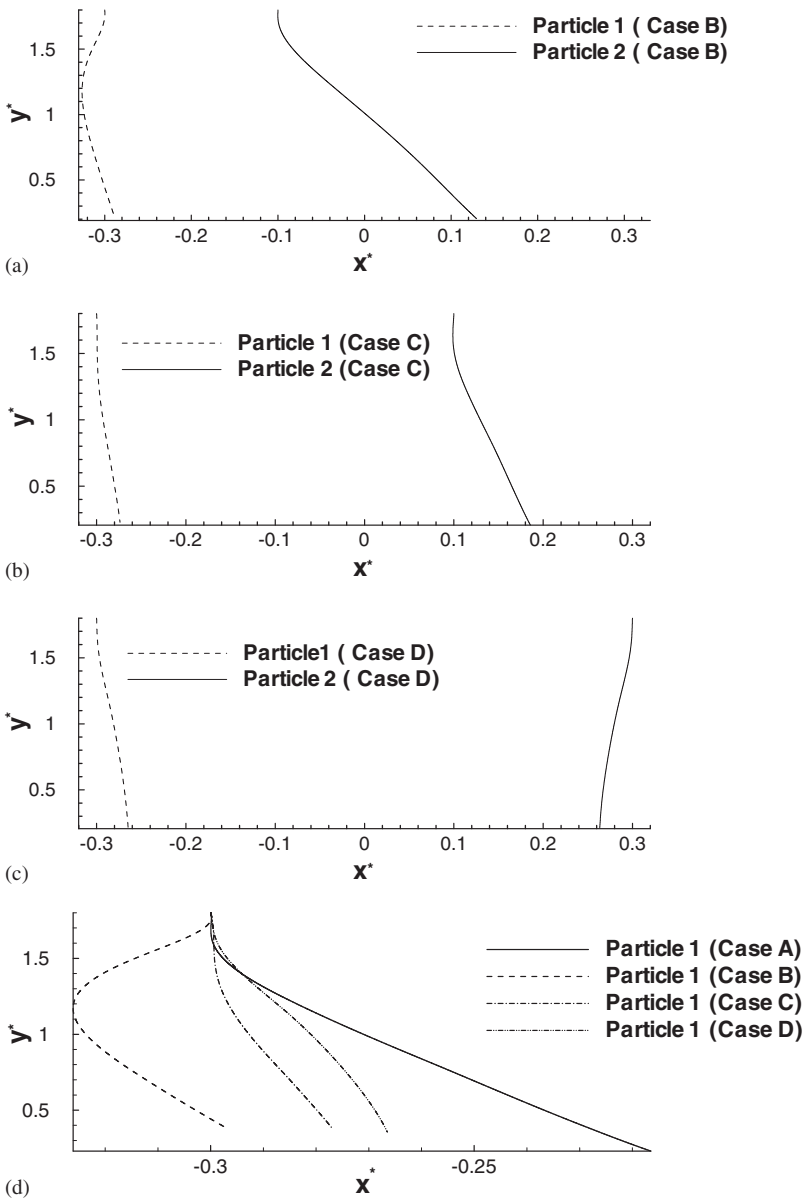

Figure 7. Paths of particle centres for: (a) Case B; (b) Case C; (c) Case D; and (d) paths of the centre of Particle 1 for Cases A–D.

studies are needed to understand whether the introduction of large particles can result in the plume breaking apart, forming two or multiple bioconvection plumes. These studies should involve multiple unit cells, which would allow investigating the effect of multiple plumes on particle sedimentation.

DOI: 10.1002/fld

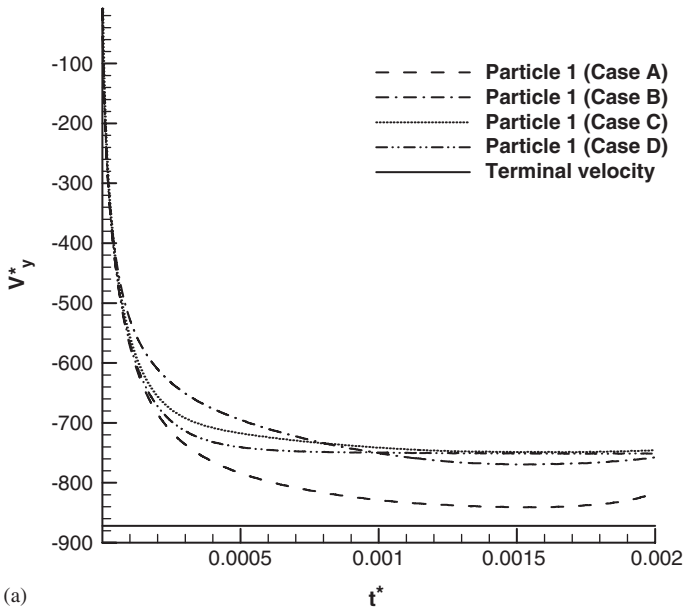

(a)

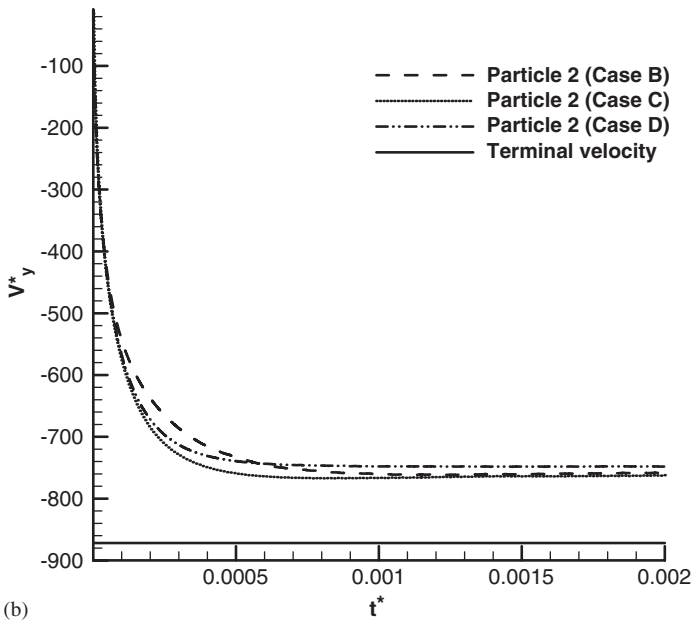

(b)

Figure 8. Dimensionless y-velocity of the particles for various cases: (a) Particle 1; and (b) Particle 2.

DOI: 10.1002/fld

ACKNOWLEDGEMENTS

AVK gratefully acknowledges grant # NAG3-2706 awarded to him by NASA Office of Biological and Physical Research, Physical Sciences Division. Constructive comments and suggestions of Mr S. M. Becker are greatly appreciated.

REFERENCES

1. Burghelea T, Segre E, Bar-Joseph I, Groisman A, Steinberg V. Chaotic flow and efficient mixing in a microchannel with a polymer solution. *Physical Review E* 2004; **69**:Art. #066305.
2. Pedley TJ, Hill NA, Kessler JO. The growth of bioconveciton patterns in a uniform suspension of gyrotactic microorganisms. *Journal of Fluid Mechanics* 1988; **195**:223–237.
3. Ghorai S, Hill NA. Development and stability of gyrotactic plumes in bioconvection. *Journal of Fluid Mechanics* 1999; **400**:1–31.
4. Ghorai S, Hill NA. Periodic arrays of gyrotactic plumes in bioconvection. *Physics of Fluids* 2000; **12**:5–22.
5. Kuusela E. *Steady-State Sedimentation of Non-Brownian Particles with Finite Reynolds Number*. Dissertation of Department of Engineering Physics and Mathematics, Helsinki University of Technology, Espoo, Finland, 2005.
6. Liu YJ, Nelson J, Feng J, Joseph DD. Anomalous rolling of spheres down and inclined plane. *Journal of Non-Newtonian Fluid Mechanics* 1993; **50**:305–329.
7. Joseph DD, Liu YJ, Poletto M, Feng J. Aggregation and dispersion of spheres falling in viscoelastic liquids. *Journal of Non-Newtonian Fluid Mechanics* 1994; **54**:45–86.
8. Singh P, Joseph DD. Sedimentation of a sphere near a vertical wall in an Oldroyd-B fluid. *Journal of Non-Newtonian Fluid Mechanics* 2000; **94**:179–203.
9. Gan H, Chang JZ, Feng JJ, Hu HH. Direct numerical simulation of the sedimentation of solid particles with thermal convection. *Journal of Fluid Mechanics* 2003; **481**:385–411.
10. Geng P, Kuznetsov AV. Settling of bidispersed small solid particles in a dilute suspension containing gyrotactic microorganisms. *International Journal of Engineering Science* 2005; **43**:992–1010.
11. Geng P, Kuznetsov AV. Introducing the concept of effective diffusivity to evaluate the effect of bioconvection on small solid particles. *International Journal of Transport Phenomena* 2005; **7**:321–338.
12. Geng P, Kuznetsov AV. Direct numerical simulation of settling of a large solid particle during bioconvection. *International Journal for Numerical Methods in Fluids* 2006; **51**:511–530.
13. Liu J-G, Wang C. High order finite difference methods for unsteady incompressible flows in multi-connected domains. *Computers and Fluids* 2004; **33**:223–255.
14. Chattot J-J, Wang Y. Improved treatment of intersecting bodies with the chimera method and validation with a simple and fast flow solver. *Computers and Fluids* 1998; **27**:721–740.
15. Houzeaux G, Codina R, Dirichlet/Neumann(Robin) coupling for the Navier–Stokes equations. *Computer Methods in Applied Mechanics and Engineering* 2003; **192**:3343–3377.
16. Pedley TJ, Kessler, JO. The orientation of spheroidal micro-organisms swimming in a flow field. *Proceedings of the Royal Society of London*, *Series B* 1987; **231**:47–70.
17. Kessler JO. The external dynamics of swimming micro-organisms. *Progress in Phychological Research*, Round, Chapman (eds), vol. 4. Biopress: Bristol, 1986.
18. Sucker D, Brauer H. Fluiddynamik bei der angeströmten Zylindern. *Wärme und Stoffübertragung* 1975; **8**:149–158.

DOI: 10.1002/fld